Statistical characterization of 60-GHz indoor radio channels

Statistical Characterization of 60-GHz Indoor Radio Channels

Peter F. M. Smulders, *Senior Member, IEEE*

Invited Paper

***Abstract*—An extensive review of the statistical characterization of 60-GHz indoor radio channels is provided from a large number of published measurement and modeling results. First, the most prominent driver applications for 60 GHz are considered in order to identify those environment types that need to be characterized most urgently. Large-scale fading is addressed yielding path-loss parameter values for a generic 60-GHz indoor channel model as well as for the office environment in particular. In addition, the small-scale channel behavior is reviewed including the modeling of time-of-arrival and angle-of-arrival details and statistical parameters related to delay spread, angular spread and Doppler spread. Finally, some research directions for future channel characterization are given.**

***Index Terms*—Angular spread, channel characterization, delay spread, Doppler spread, indoor radio channel, millimeter-wave propagation, multipath channels, path loss, 60 GHz, statistical characteristics, wideband channel measurement.**

I. Introduction

In recent years, considerable attention has been devoted to the design and standardization of multi-Gbps wireless systems operating in the 60-GHz band for a large variety of low-cost consumer applications [1]–[7]. When compared with the conventional systems operating in the lower frequency bands, e.g., 2.4 GHz, a significant additive challenge is the achievement of sufficient linkbudget. The main reasons for this are the much lower performance of the low-cost (silicon-based) RF-sections as well as the much higher propagation loss as shown in [8]. On the other hand, it is easier to establish highly focused antenna beams at both ends of the link by means of yet small antenna structures. In this manner, the lower RF performance and higher propagation losses can be compensated by a high antenna gain. Consequently, in the context of 60-GHz radio design, a paradigm-shift has occurred from omnidirectional radios to beam-forming radios. Proper design of such link-budget critical radios requires reliable statistical path-loss models as well as reliable statistical modeling of channel impulse response details such as angle-of-arrival distributions.

Manuscript received May 04, 2009; revised July 17, 2009. First published August 18, 2009; current version published October 07, 2009. This work has been carried out as part of the MEDEA+ project Q-Stream.

The author is with the Eindhoven University of Technology (TU/e), Eindhoven, The Netherlands (e-mail: p.f.m.smulders@tue.nl).

Color versions of one or more of the figures in this paper are available online at http://ieeexplore.ieee.org.

Digital Object Identifier 10.1109/TAP.2009.2030524

Let us consider the foreseen 60-GHz driver applications in order to identify the indoor environment types that have to be characterized most urgently. There are three applications of particular interest: The first one is (multiple) uncompressed high definition video streaming as explicitly targeted by the wirelessHD standardization consortium [5]. The second one is ultra-fast wireless LAN which is the focus of the very high throughput (VHT) consortium [7] and the third one is ultra-fast downloading including "Kiosk file downloading" as proposed by the consortium for millimeter-wave practical applications (CoMPA) [3], [4]. The first mentioned application and the third one comply with the two usage models that are selected by the IEEE 802.15.3 Task Group 3c as mandatory for physical layer simulations [9], [10]. Note, that these three mentioned applications are all typically for indoor use. Therefore, we restrict ourselves to indoor environments. Obviously, the uncompressed high definition video application calls for characterization of the residential environment. In addition, the wireless LAN application and the fast downloading application necessitate the characterization of the office environment. The first two applications need to operate under line-of-sight (LOS), as well as under non-line-of-sight (NLOS) conditions at a transmit-receive (Tx-Rx) distance of maximally 5 m, whereas fast downloading needs only to operate in a LOS situation with a Tx-Rx distance of 1 m at maximum.

For the channel characterization of these most prominent usage models and corresponding indoor environments we consider the fading of received power which can be decomposed into two parts: large-scale fading and small-scale fading and which is given by

$$P_{\mathrm{inst}}(d) = P_{\mathrm{large}}(d) + P_{\mathrm{small}}(d) \quad [\mathrm{dB}]. \tag{1}$$

Here, the large-scale fading at Tx-Rx distance d, $P_{\mathrm{large}}(d)$, describes the average behavior of the channel, mainly caused by the free space path loss and the blocking effect of large objects, while the small-scale fading at distance d, $P_{\mathrm{small}}(d)$, characterizes the signal change in a local area within a range of only a few wavelengths. The small-scale fading is obtained merely by subtracting the large-scale fading from the instantaneous fading $P_{\mathrm{inst}}(d)$ in dB. In Section II, we will address the large-scale characterization, i.e., path loss, relevant for the aforementioned applications. In Section III, we will address the characterization of small-scale effects, i.e., time and spatial dispersion as well as the channel dynamics that results from this dispersion and time variability as a result of movement and displacements in the channel. Finally, in Section IV, a summary and the conclusions are presented.

TABLE I
PATH-LOSS PARAMETER VALUES OBTAINED FROM MEASUREMENTS

Environment	LOS/NLOS	HPBW [degrees] Tx	HPBW [degrees] Rx	$L(d_0)$ [dB] (d_0= 1 m)	n	Ω [dB]	Ref.
conference	LOS	80 – 120	10	46	1.6	1.6	[13]
conference	LOS	10	10	34	1.7	1.5	[13]
conference	LOS	80 – 120	80-120	60	1.5	1.5	[13]
corridor	LOS	80 – 120	80-120	57	2.0	0.14	[13]
various	LOS+NLOS	90 – 125	7 – 56	69	1.88	8.6	[14]
computer	LOS	30	30	45.47	1.92	1.72	[15]
office/conf.	LOS+NLOS	360	360	70	1.33	5.1	[16]
corridor	NLOS	9.1 – 9.8	360 – 11		1.64	2.53	[17]
office/hall	LOS	9.1 – 9.8	360 – 11		2.17	0.88	[17]
office/hall	NLOS	9.1 – 9.8	360 – 11		3.01	1.55	[17]
conference	LOS	360 – 70	360 – 70	68.6	1.33	0.79	[18]
laboratory	LOS	360 – 9	360 – 9	68.3	1.2	2.7	[19]
laboratory	NLOS	360 – 9	360 – 9	34.8	5.4	3.9	[19]
office	LOS	360	360		2.1		[20]
office	NLOS	360	360		3.5		[20]
laboratory	LOS	58	58	56.12	2.5	2.0	[21]
laboratory	LOS	58	58	58.99	2.3	2.4	[21]
laboratory	LOS	58	12	40.26	2.1	1.8	[21]
laboratory	LOS	58	12	44.93	1.9	2.3	[21]
corridor	LOS	120	120	74.05	1.88		[22]
corridor	LOS	120	15	59.65	1.87		[22]
office	LOS	360	360		1.67		[23]
various	LOS+NLOS	8	8		2.1	7.9	[24]
residential	LOS	72	60	75.1	1.53	1.5	[25]
residential	NLOS	72	60	86.0	2.44	6.2	[25]
office	LOS	30	30	84.6	1.16	5.4	[25]
office	NLOS	30	30	56.1	3.74	8.6	[25]
residential	LOS	60	10		1.73	1.6	[26]
office	LOS	72	60		0.56	1.2	[26]

II. CHARACTERIZATION OF LARGE-SCALE EFFECTS

Commonly, the large-scale channel fading is characterized by the log-distance path-loss model given by

$$L(d) = L(d_0) + 10 \cdot n \cdot \log_{10}\left(\frac{d}{d_0}\right) + X_\Omega \quad [\mathrm{dB}]$$
$$= \overline{L}(d) + X_\Omega \quad [\mathrm{dB}] \tag{2}$$

where $L(d)$ represents the path loss in decibels at separation distance d, $L(d_0)$ is the reference path loss at some reference distance d_0, n is the path-loss exponent and X_Ω represents the shadowing component which is assumed to be a zero mean Gaussian distributed random variable with a standard deviation Ω [11], [12]. $\overline{L}(d)$ represents the average path loss.

Path loss can be determined by taking

$$L(d) = P_\mathrm{T} - \overline{P}_\mathrm{R}(d) + G_\mathrm{T} + G_\mathrm{R} \quad [\mathrm{dB}] \tag{3}$$

in which $\overline{P}_R(d)$ represents the average of a large number of received power values measured within an area of only a few wavelengths at distance d of the transmit antenna which transmits with power P_T. The averaging is done to average out the small-scale variations. G_T and G_R are the antenna gain values of the Tx and Rx antenna, respectively, which are assumed to be aligned in each others line-of-sight direction. An undesirable effect of calibrating out the influence of the antennas in this way is that the influence of the environment, which we want to capture, becomes masked because of the spatial filtering effect of the antenna gain functions. This effect can be minimized by using highly omnidirectional antennas. However, it is also interesting to know the path-loss characteristics experienced with highly directional channels since directional antennas are certainly required to gain sufficient link budget for the support of the envisioned high data rate services [2]. Therefore, we consider measurement and modeling results obtained with highly omnidirectional as well as with highly directive antennas. Table I lists values of the path loss parameters $L(d_0)$, n and Ω based on extensive measurement campaigns which have been performed in a large variety of indoor environments under LOS as well as NLOS conditions as reported in [13]–[26]. In all cases, the reference distance d_0 is taken 1 m. In addition, the half-power beamwidth (HPBW) in the azimuth direction of both the Tx and the Rx antenna are given in order to examine the relationship between antenna beamwidth and the obtained path-loss values. All these measurements have been performed in the 57–65 frequency band except those reported by [13] which have been done in the 67–72 band.

When considering the values of $L(d_0)$ for $d_0 = 1$ m we observe a striking spread in values from 34 to 86 dB. At 60 GHz, the wavelength in free space amounts to $\lambda = 5$ mm and according to the Friss free-space law we would expect values close to $20\log(4\pi/\lambda) = 68\,\mathrm{dB}$ for LOS situations (assuming far-field conditions) since at the short Tx-Rx distance of 1 m a dominant LOS component is expected when compared with the multipath reflections. Part of the explanation is that in many cases antenna gain values are not calibrated out according to (3) resulting in much lower values of $L(d_0)$. Also, additional losses like those occurring in the waveguides between antennas and measurement equipment might not be taken into account. Unrealistic values of $L(d_0)$ may also occur due to extrapolation of the linear fits of measurement results taken at much larger distances.

TABLE II
AVERAGE PATH-LOSS EXPONENT $\overline{n}$ AND AVERAGE STANDARD DEVIATION $\overline{\Omega}$ FOR DIFFERENT ENVIRONMENTS

Environment	LOS/NLOS	$\overline{n}$	$\overline{\Omega}$
offices	LOS	1.6	1.8
laboratories	LOS	2.0	2.24
corridors	LOS	1.92	0.14
residential	LOS	1.53	1.5
offices	NLOS	3.4	5.1
laboratories	NLOS	5.4	3.9
corridors	NLOS	1.64	2.53
residential	NLOS	2.44	6.2

Another cause of considerably deviating values is antenna misalignment which can cause a significant drop of received power in particular at small distances. The most realistic model value of $L(d_0)$ is, therefore, the one based on the Friss free-space law, i.e., 68 dB for LOS. For NLOS the Friss free-space law does not apply so that the $L(d_0)$-value for NLOS remains inconclusive.

The values for n and Ω in Table I show that it makes much sense to differentiate between the LOS scenarios and NLOS scenarios: for the LOS case the values for n are around 1.7 whereas NLOS values are 3.5 on average. The difference also becomes clear when considering the spread in values as expressed by the Ω-values: 2.1 on average for the LOS case and 4.6 for NLOS. If values obtained in different environments are considered together to determine one single value of Ω, then one can expect a high value because the differences in environment will contribute to the spread in values. This explains the high Ω-values for "LOS + NLOS".

In order to obtain an impression of the influence of antenna beamwidth on the path loss parameters we classify an antenna as "directional" in case the HPBW of its beam is 30° at maximum. Otherwise the antenna is considered to be "omnidirectional". Furthermore, we classify a "directional channel" as a channel with a directional antenna applied at one side of the link or at both sides of the link. If "omnidirectional" antennas are applied at both sides, then the channel is considered to be an "omnidirectional channel".

Application of this 30°-beamwidth criterion on the parameter values given in Table I reveals that the average of all n-values obtained under LOS conditions amounts to 1.79 for the directional channels and 1.69 for omnidirectional channels. For NLOS, these figures amount to 2.80 and 3.78, respectively. So, for LOS as well as for NLOS the average values of n are quite similar. This also accounts for $L(d_0 = 1)$ and Ω-values. This indicates that a differentiation between omnidirectional channels and directional channels is not needed.

A good impression of the influence of the environment can be obtained by grouping the results in Table I for office rooms (including conference rooms), laboratory rooms, corridors and residential environments. Table II shows the average values for these four groups with differentiation between LOS and NLOS.

From Table II, it occurs that, on average, there is not a striking difference in parameter values between the groups. For all environments we observe significantly larger average values for NLOS when compared with the values obtained under LOS conditions with exception of the low average path-loss exponent found for corridors and NLOS. The overall similarity of results indicates that it would be well possible to define a generic path-loss model by averaging the reported results. Based on the averaging of the large set of values given in Table I we propose a generic indoor path-loss model for the 60-GHz band according to (2) with path-loss parameters values for the LOS-case as well as for the NLOS-case as listed in Table III. Based on the averaging of the smaller set of values obtained for office rooms including conference rooms and a computer room, we propose the parameter values listed in Table IV. This set of parameter values for the office room may be considered as a refinement which, e.g., excludes the typical low NLOS values for the path-loss exponent found in corridors. Note the resemblance of parameter values between the generic model and the office-room model. This confirms that the generic model has a good validity for a more specific environment such as an office room and, on the other hand, it indicates that the office-room environment typically represents a large variety of indoor environments.

TABLE III
PARAMETERIZATION OF GENERIC 60-GHz PATH-LOSS MODEL FOR INDOOR ENVIRONMENTS

	$L(d_0)$ [dB] ($d_0 = 1$ m)	n	Ω [dB]
Generic LOS	68.0	1.7	1.8
Generic NLOS	-	3.3	4.6

TABLE IV
PARAMETERIZATION OF 60-GHz PATH-LOSS MODEL FOR OFFICE ENVIRONMENTS

	$L(d_0)$ [dB] ($d_0 = 1$ m)	n	Ω [dB]
Office LOS	68.0	1.6	1.8
Office NLOS	-	3.4	5.1

It occurs that, under LOS circumstances, values of n are typically below the free-space value $(n = 2)$. This can be explained by a phenomenon that is commonly denoted as the "wave-guide effect": at small Tx-Rx distances, the reflected waves are partly rejected by the spatial filtering of the directive antennas whereas at larger distances the reflected waves contribute more to the average received power since they are better aligned with the antennas. This is a well-known effect that can be observed for much lower frequencies as well. The values of n observed at 60 GHz are quite similar to those found for conventional mobile radio frequencies which are 1.6–1.8 for LOS and 4–6 for NLOS [27]. It follows from (2) that, for the maximum Tx-Rx distance of 5 m, the model value of parameter $n = 1.7$ implies a link-budget advantage of 2 dB in comparison with the free-space assumption of $n = 2$.

As noted in the introduction, it is also highly necessary to make a similar path-loss characterization of the residential indoor environment based on measurement data as reported in [25] taking into account the influence of furniture in typical residential environments as addressed in [28].

All path-loss results in Table I have been obtained with application of linearly polarized antennas. However, path-loss parameters obtained with circular polarization are also reported [15]. Under LOS conditions, a path-loss exponent of $n = 1.61$ was found for circular polarization whereas $n = 1.92$ was

found for linear polarization with exactly the same LOS measurement setup. This lower value for n is an interesting result and can be explained by the fact that circular polarization tends to cancel the odd-times reflected rays: at a small TR distance, all reflected rays are extra attenuated by the circular polarization because they are all single reflections whereas at larger distances a large amount of reflections are not extra attenuated because they are even-time reflected rays. In that way, circular polarization might magnify the formerly mentioned wave-guide effect. A lower path-loss exponent suggests that the received power decreases less rapidly with respect to the Tx-Rx distance so that circular polarization would permit a better radio coverage in the indoor environment. Unfortunately, this reduction of large-scale fading is only obtained under LOS conditions. In NLOS scenarios, the link has to relay on reflected paths due to the high blocking effect of objects that obstruct the direct LOS path as demonstrated in [29]–[31]. At the moment the LOS path becomes blocked a beam-steering 60-GHz radio will try to maintain the link by directing the antenna beam towards the best alternative path which will be typically a strong, single-reflected ray. The use of circular polarization would cancel this first alternative and the radio has multiple-reflected rays as alternative which would considerably jeopardize the radio performance. On the other hand the likely use of array antennas that produce linearly polarized waves may yield a rather undefined direction of polarization at the receiving end which may lead to a considerable polarization loss. These kind of polarization issues deserve substantial consideration in channel characterization work.

III. Characterization of Small-Scale Effects

Small-Scale effects occur from interaction of complex impulse-response details as observed within a limited bandwidth. Complex impulse responses obtained in the 60-GHz band are typically ray like and can be expressed as a temporal-spatial discrete multipath model as follows:

$$h(\tau;t)=\sum_n \beta_n(t)e^{j2\pi f_n(t)}\delta\left(\tau-\tau_n(t)\right)\delta\left(\phi-\phi_n(t)\right) \quad (4)$$

where β_n, f_n, τ_n and ϕ_n represent the amplitude, frequency, delay and angle-of arrival of ray n, respectively. $\delta(\cdot)$ denotes the Dirac delta function. Note, that τ represents excess delay whereas the t-dependence represents the changes with time of the very structure of the impulse response. A realistic assumption is that, per measurement subset, all responses considered are generated according to the same statistical process and that the real part and imaginary part of the ray phasor at each particular excess delay cross section are identically distributed variables. An additional realistic assumption is that the ray generation process is a wide-sense stationary process with respect to the t variable [32]. The process $\mathrm{h}(\tau;t)$ is not stationary with respect to the τ variable and, thus, nonergodic. If furthermore uncorrelated scattering is assumed, which means that the signals coming from different paths experience uncorrelated attenuations, phase shifts and time delays, the channel is said to be a wide-sense stationary uncorrelated scattering (WSSUS) channel. In that case, the theory of linear time-variant filters applies [33]. The WSSUS channel characterization is appropriate for describing the small-scale behaviour of the channel which is suitable and sufficient for the air interface design of a digital communication system [34]. A convenient way is to describe the WSSUS channel as a tapped delay line. Tapped delay line models for 60-GHz channels are proposed in [35] and [36]. In what follows, we will address the characterization of Doppler spread caused by the differences in ray frequency, delay spread caused by the differences in ray delay τ_n, and angular spread caused by the differences in ray angle-of-arrival ϕ_n, respectively.

A. Doppler Spread

Coherence Time: The transmission channel can vary over time due to movements of objects and persons in the environment or moving antennas at the transmitter and/or receiver which results in a spectrum broadening. When the angles of arrival of the multipath components are uniformly distributed in all directions in the horizontal plane, a "U"-shaped Doppler spectrum occurs, that is well known as the Clarke's model [37]. In the case of 3-D scattering, which might be more realistic to occur in an indoor environment, it is shown that the Doppler spectrum of the received signal is uniform over the full range of Doppler frequencies centered on the carrier [38]. In both cases, the coherence time T_{coh} is approximately the inverse of the Doppler spread $2f_{\mathrm{D}}$, where f_{D} is the maximum Doppler frequency

$$T_{\mathrm{coh}}\approx\frac{1}{2f_D}. \quad (5)$$

The minimum coherence time due to movements of people in a typical indoor environment for a carrier frequency $f_{\mathrm{c}}=60$ GHz and a maximum walking speed of 1 m/s can be obtained as follows: a ray reflecting from a person having this speed may experience a Doppler shift of $f_D=2f_c\cdot v/c=400$ Hz (with c the velocity of electromagnetic waves in vacuum). Hence, the presence of many persons moving at various speeds up to 1 m/s results in a Doppler spread of about 800 Hz and, equivalently, a coherence time of about 1 ms. This is the absolute lower limit which might be approached when omnidirectional antennas are used. If directional antennas are used instead of omnidirectional, some or many fading contributions are minimized by the spatial filtering effect of the antenna patterns resulting in a higher coherence time. Results of Doppler spread and coherence-time measurements obtained at 60 GHz with highly directional antennas are reported in [39] and [40], respectively. Doppler analysis, which was performed when people were moving inside a laboratory room, revealed a maximum observable Doppler frequency of 200 Hz and a Doppler spread of 150 Hz [39]. In [40], the situation was studied in which people walked along the line-of-sight path while not obstructing it, with a maximum walking speed of 1.7 m/s. The minimum observed coherence time was 32 ms which is indeed much higher than the lower limit of 1 ms.

Channel Dynamics: The fading experienced is termed "slow fading" with respect to the data stream in case the symbol time $T_s\ll T_{\mathrm{coh}}$. Slow fading, and, thus, an essentially static channel, is experienced if the symbol rate $r_s\gg T_{\mathrm{coh}}^{-1}=1$ ksps. For the envisioned Gbps applications the channel can be estimated once

per many thousands of data symbols (and for directional channels even once per ten-thousands of data symbols). Thus, Gbps radios operating at 60 GHz will encounter slow fading despite of their high carrier frequency because of the slow speeds of displacement in indoor environments and the high data rates at which these radios operate. Hence, the 60-GHz channel can be considered as a static channel which justifies the elimination of the t-dependence in (4).

B. Delay Spread

Single-Cluster Time-of-Arrival Model: Reflected rays may be composed of many different components which add up within the measurement resolution. This is because in many cases the reflecting wall and objects have a layered and/or irregular structure at a scale smaller than (or comparable with) the measurement resolution. A wideband channel sounder with a bandwidth of 2 GHz and a "normal" window has a resolution of 1 ns which complies with 30 cm. According to the Central Limit Theorem, the real part as well as the imaginary part of a ray phasor that is built up of many random components is Gaussian distributed. This, together with the reasonable assumption of uniformly distributed ray phases, results in the assumption that the amplitudes $\beta_{\rm n}$ follow a Rayleigh distribution. The validity of this assumption has been confirmed by means of the chi-squared goodness-of-fit test [32]. Therefore, we propose to model the ray amplitude distribution as a Rayleigh distribution. The Rayleigh model is confirmed by [16] for office and residential environments under LOS conditions using 5-GHz bandwidth.

The Rayleigh parameter for each ray, i.e. the average power $\overline{\beta_n^2}$ for a ray at excess time τ_n has been modeled as

$$\overline{\beta_n^2} = \begin{cases} \overline{\beta_0^2}, & \text{if } \tau_n = 0 \\ \Pi, & \text{if } 0 > \tau_n \geq \tau_c \\ \Pi \cdot e^{-\gamma(\tau_n - \tau_c)}, & \text{if } \tau_n \geq \tau_c. \end{cases} \tag{6}$$

For LOS situations, $\overline{\beta_0^2}$ will be typically much larger than Π whereas for NLOS, $\overline{\beta_0^2}$ becomes much smaller and can be modeled as being zero. This model was first proposed in [32] and further developed in [41]. The constant level part comes from antenna misalignment. The model parameters $\overline{\beta_0^2}$, γ, and $\tau_{\rm c}$ highly depend on antenna directivity and misalignment. This dependence is addressed in [19]. With perfectly omnidirectional antennas or perfectly aligned antennas $\tau_{\rm c}$ approaches zero which corresponds to the classical exponentially decaying profile.

Interarrival times pdf's obtained from a large set of measurements have been subjected to a chi-squared test. Unfortunately, this test failed to yield results of sufficient significance. This was mainly caused by the limited number of interarrival time classes, though the total number of values was considerable, typically several thousand values per measurement subset. However, good correlation coefficients (MMSE) between exponential fit and empirical frequency distributions have been found which implies that the ray arrival process approximates a Poisson process, i.e., the pdf of ray interarrivals is approximately exponential.

Multicluster Time-of-Arrival Model: The observation that the ray interarrival time process is not exactly a Poisson process can be explained by ray clustering. Measurement results confirm this clustering and some indicate that the arrival rate is larger for clusters that arrive later in time [42]. A well-known discrete impulse response model that takes ray-clustering into account is the Saleh-Valenzuela (S-V) model [43] which is given by

$$h(\tau) = \sum_{l=0}^{L-1} \sum_{k=0}^{K_l - 1} \beta_{k,l} e^{j\theta_{k,l}} \delta(\tau - T_l - \tau_{k,l}) \tag{7}$$

in which L is the number of clusters, $K_{\rm l}$ is the number of rays in the lth cluster, $\beta_{\rm k,l}$ and $\theta_{\rm k,l}$ are the amplitude and phase of the kth ray in the lth cluster, $T_{\rm l}$ is the arrival time of the first ray of the lth cluster and $\tau_{\rm k,l}$ is the delay of the kth ray within the lth cluster relative to $T_{\rm l}$ with $\tau_{0,\rm l} = 0$ and $T_0 = 0$.

The cluster arrival rate as well as the ray arrival rate are modeled as a Poisson process so it is assumed that all clusters have the same ray arrival rate. According to the S-V model the clusters decay exponentially and also the rays within each cluster have an exponential decay

$$\overline{\beta_{k,l}^2} = \overline{\beta_{0,0}^2} e^{-T_l/\Gamma} e^{-\tau_{k,l}/\gamma} \tag{8}$$

where $\overline{\beta_{0,0}^2}$ is the average power of the first ray of the first cluster. Γ and γ are the cluster decay factor and the ray decay factor, respectively. For the 60-GHz band, values of these parameters have been proposed in [44]. In the original S-V model the ray amplitudes have a Rayleigh distribution. As already noted, this is also found for high-resolution measurement with bandwidths of 2–5 GHz. However, also a log-normal distribution is used to model the ray amplitudes [25].

RMS Delay Spread: The most commonly used statistical parameter to describe the time-domain dispersion of a radio channel is the root mean square delay spread (RDS) which is the second moment of the PDP [32]. RDS highly depends on HPBW of the applied antennas. This dependence is shown in Fig. 1 which depicts RDS as function of travel distance of the first arrived ray (which equals Tx-Rx distance in the case of LOS) for various combinations of omnidirectional antenna as decribed in [45] (HPBW is 360° in azimuth and 9° in elevation), fan-beam antenna (HPBW is 70° in azimuth and 12° in elevation) and pencil-beam antenna (HPBW is 8.3° in both azimuth and elevation) [19].

Fig. 1(a) depicts RDS results obtained with omnidirectional antennas at both ends under LOS as well as NLOS conditions and at various antenna heights which are indicated in the legend.

The LOS area corresponds to a Tx-Rx distance of the first arrived path smaller than 6.2 m, whereas the NLOS area corresponds to a travel distance of the first arrived reflected path in excess of 7.9 m.

Fig. 1(b) shows results obtained with various combinations of different antennas in LOS situations. The Tx antenna was a fan-beam antenna positioned at 2.4-m height with the fan beam directed towards the middle of the room. Measurements have been performed with all three antenna types at the Rx side. The setup with the omnidirectional antenna at the Rx side is denoted in the legend as "Fan-Omn". The fan beam and pencil beam were directed towards the Tx antenna without any pointing error (denoted by "Fan-Fan" and "Fan-Pen", respectively) and with a pointing error in the azimuth plane of ± 35 degrees (denoted by "Fan-Fan 35° dev." and "Fan-Pen 35° dev.", respectively).

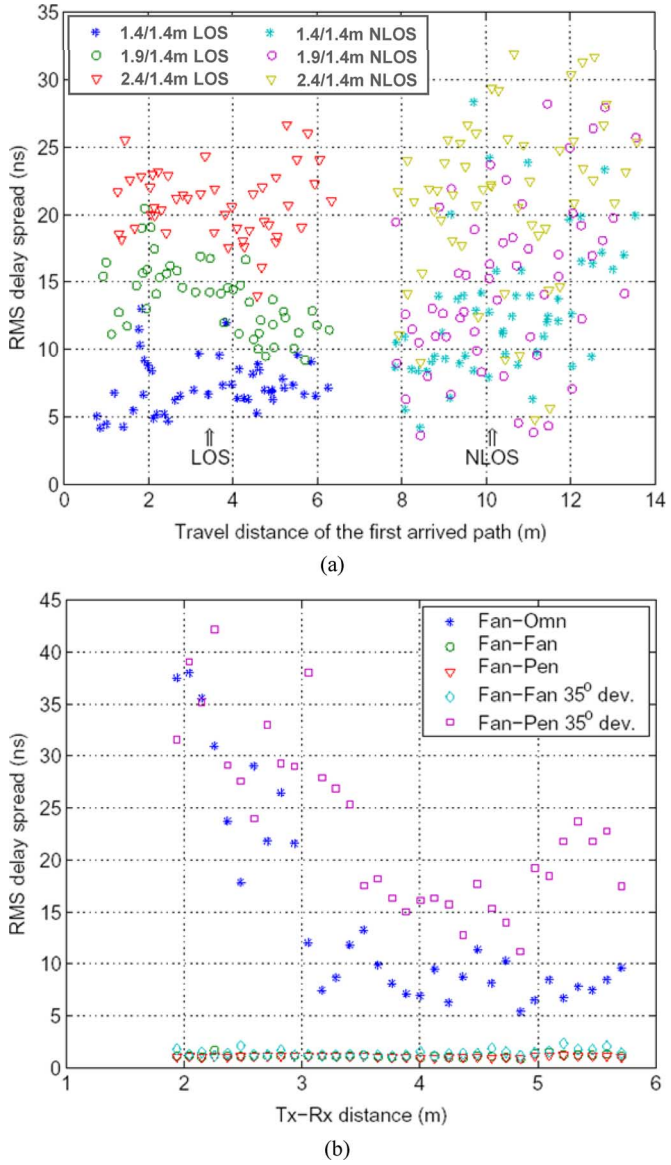

Fig. 1. RMS delay spread as function of Tx-Rx distance for different antenna configurations: (a) with omnidirectional Tx antenna and omnidirectionl Rx antenna at various antenna heights as indicated in the legend (Tx height/Rx height in meters) for LOS and NLOS (b) with fan beam at Tx at 2.4-m height and omnidirectional antenna, fan-beam antenna, and pencilbeam antenna at 1.4-m height for LOS. For Rx fan beam and Rx pencil beam also the results with 35° of pointing error are given.

It is striking to observe that RDS can be reduced so easily to about 1 ns by using high gain antennas. With the fan-beam antennas at both sides it is even possible to get such a low delay spread with 35° degrees of mispointing. This means that, with these type of antennas, reliable transmission with data rates in the order of Gbps can be obtained with very simple basic modulation schemes such as binary amplitude shift keying! With omnidirectional antennas, however, RDS values reach typically higher values depending on room size and reflectivity of the environment; up to 15 ns for small-sized offices (8 m^2 and 12m^2) and up to 6 ns is found for a residential environment [16]. This relatively low value is explained by the absorptive furniture (couches, carpets, etc.) unique to the private home

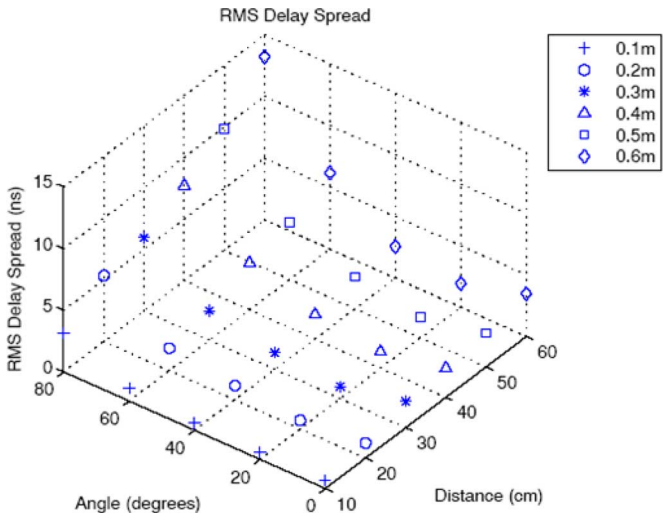

Fig. 2. RMS delay spread as function of misalignment angle and Tx-Rx distance.

environment. RDS values found in larger office rooms (85 m^2 to 105 m^2) are typically between 15 and 45 ns [32], [46].

For small Tx-Rx distances (<1 m) not many RDS or coherence bandwidth results are reported although those could be highly significant for at least one important target application and that is high-speed download; the short distance in combination with LOS availability makes this application relatively simple to implement (when compared with uncompressed-HD streaming video and ultra-fast wireless LAN which have to operate at much larger Tx-Rx distances and under NLOS conditions) since one important bottle-neck problem does not exist and that is the stringent link-budget requirement. Antennas can be relatively simple without any, or with only a simple form of, beam-steering or switching. Furthermore, the dominant LOS at those short distances will reduce the RDS considerably so that modulation schemes with low complexity can be possibly applied. Because of the significance of this we present some original RDS results obtained in an office environment. The antennas are both open waveguides which have a HPBW of 80° in azimuth and 90° in elevation. RDS values have been measured at different Tx-Rx distances and under different misalignment angles in the azimuth plane. The results are shown in Fig. 2. The angle of 0 degrees complies with perfect alignment.

Fig. 2 shows that RDS values consequently decrease with decreasing Tx-Rx distance. RDS values also decrease with decreasing azimuth angle except for azimuth angle 0. This can be explained as follows: with the decrease of the azimuth angle the RDS becomes smaller since the antennas become better aligned but as soon as the alignment becomes perfect the RDS increases as a results of multiple reflections between the transmit and receive unit which both have metal fronts of about one square decimeter. If one of the antennas is turned around its (waveguide) axis by 90 degrees, RDS increases, e.g., to 13.2 ns at a Tx-Rx distance of 30 cm. In addition, the received signal power decreases significantly due to the large polarization mismatch. The application of circular polarization will presumably solve this problem of critical antenna orientation. In addition, circular polarization will reduce delay spread because odd-time reflected

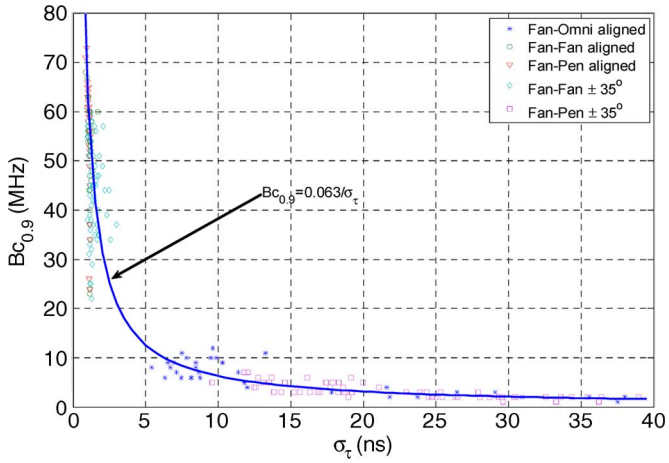

Fig. 3. Coherence bandwidth versus RMS delay spread values for different antenna configurations: with fan-beam at Tx at 2.4-m height and omnidirectional antenna, fan-beam antenna, and pencil-beam antenna at 1.4-m height for LOS. For Rx fan beam and Rx pencil beam also the results with 35° of pointing error are given.

rays are largely attenuated. Ref. [47] reports a reduction in RDS to about half the values found for linear polarization.

Coherence Bandwidth: The coherence bandwidth $B_{\mathrm{coh},0.9}$ can be defined as the frequency shift where the correlation level falls below 0.9. So, within that range two frequency points have a strong correlation. Fig. 3 shows scatter plots of the coherence bandwidth versus RDS values obtained in two office rooms with antennas configurations corresponding to those from Fig. 2(b) [48].

The relationship between $B_{\mathrm{coh},0.9}$ and RDS is obtained by least-square fitting the scatter points in Fig. 3 for all the configurations yielding

$$B_{\mathrm{coh},0.9} = \frac{0.063}{\sigma_\tau}. \tag{9}$$

The factor value of 0.063 complies very well with the one found for offices, library and laboratory (0.06) [16] and also with the average value of 0.063 found for a conference room [18]. In [35], a much larger value is reported (0.285) but large part of these measurements were performed in two long and narrow corridors which are not representative at all for office rooms.

K-Factor: The Ricean K-factor is defined as the ratio between the powers contributed by the dominant path and the scattered paths. The K-factor of a Ricean channel delay profile is strongly related to the RDS; it tends to increase with decreasing RDS. For the special case of an exponentially decaying power delay profile, the K-factor and RDS are related by $\sigma_\tau \cdot K' = 1/\gamma$ with $K' = (K+1)/\sqrt{2K+1}$ and γ the decay exponent of the decaying part [48]. This implies that, next to RDS, also the K-factor strongly depends on the antenna gain functions. This is shown in Fig. 4(a) and (b), which shows the K-factor values that correspond to the RDS values depicted in Fig. 1(a) and (b), respectively [19].

C. Angular Spread

- Some illustrative angle-of-arrival (AoA) measurements have been performed in a typical office room to examine the effectiveness of beam switching [49]. Fig. 5 shows the normalized received power, i.e., the total received power

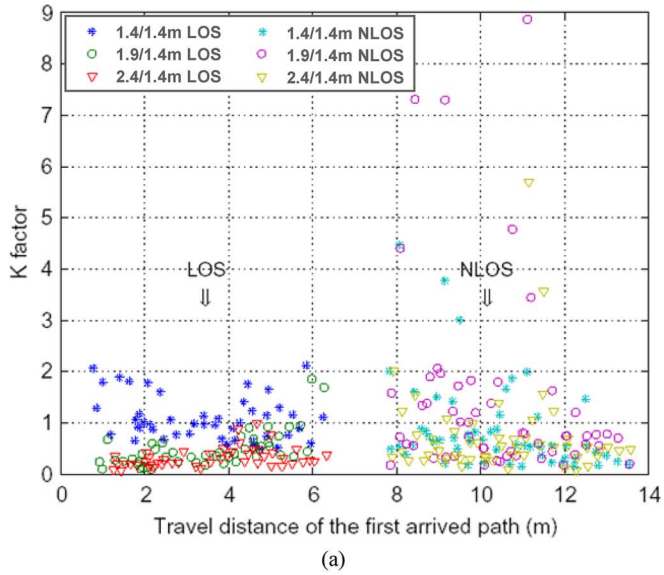

(a)

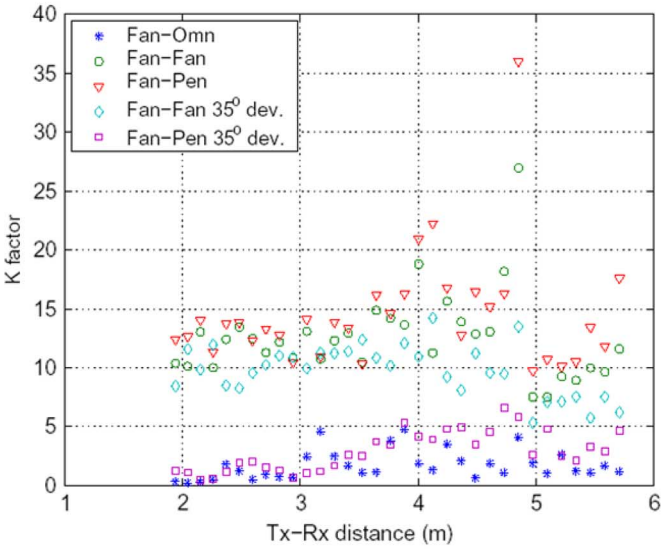

(b)

Fig. 4. Ricean K-factor as function of Tx-Rx distance for different antenna configurations: (a) with omnidirectional Tx antenna and omnidirectionl Rx antenna at various antenna heights as indicated in the legend (Tx height/Rx height in meters) for LOS and NLOS (b) with fan beam at Tx at 2.4-m height and omnidirectional antenna, fan-beam antenna, and pencil-beam antenna at 1.4-m height for LOS. For Rx fan beam and Rx pencil beam also the results with 35° of pointing error are given.

normalized on the transmitted power, versus Tx-Rx distance. The Tx antenna was the aforementioned fan-beam antenna pointing towards the middle of the room whereas the Rx antenna was the aforementioned omnidirectional antenna (both LOS and NLOS situations considered) or fan-beam antenna (only LOS situations considered). For the Rx fan-beam antenna different pointing errors were considered as indicated in the legend of Fig. 5. As expected, the best performance is obtained under LOS conditions with the Rx fan beam antenna precisely pointed towards the Tx antenna. Now let us assume that a five-sector antenna switches towards the one but best sector as soon as the LOS becomes blocked. From Fig. 5 it can be observed that the received power then drops typically 5 to 10 dB and as such the received power level becomes

similar to the level obtained with an omnidirectional antenna despite the much lower antenna gain. Obviously, the omnidirectional antenna has a much better capability to collect reflected power from its environment than the fan-beam antenna. In addition, antenna misalignment is not an issue. This indicates that simple beam switching is not so effective and that only fine beam steering will significantly outperform simple static omnidirectional antennas. This implies that sophisticated measurement and modeling of AoA on top of ToA is required to allow optimization of beam steering requirements and algorithms. It also indicates that, when applying directional antennas, misalignment is an issue and antenna beam shapes have to be optimized in this respect as illustrated in [50] and [51]. According to [52], a beam steering gain of over 8 dB can be achieved with 90% probability.

- *Angle of Arrival modified S-V model*: In addition to spread and clustering in the time domain also spread and clustering in the angular domain has been observed [13], [14], [49], [53]–[55]. The S-V model was extended by [53] to include the AoA statistics as follows:

$$h(\tau) = \sum_{l=0}^{L-1} \sum_{k=0}^{K_l-1} \beta_{k,l} e^{j\theta_{k,l}} \delta(\tau - T_l - \tau_{k,l}) \delta(\phi - \Psi_l - \psi_{l,m}) \tag{10}$$

where $\Psi_{\rm l}$ and $\psi_{\rm l,m}$ represent the angle of arrival in the azimuth plane of the each cluster and the angle of arrival of the mth ray related in the lth cluster, respectively. The distribution of the angle is assumed to be a Laplacian distribution [56], [57]

$$p(\psi_{l,m}) = \frac{1}{\sqrt{2}\sigma_\phi} e^{-\sqrt{2}\psi_{l,m}/\sigma_\phi} \tag{11}$$

where σ_ϕ is the angular-spread of rays in the lth cluster.

Results of angular spread measurements are reported in [25] and [57]. For a residential environment and under LOS conditions, values are 49.2°, 119°, 46.2°, and 107° for a Tx HPBW of 360°, 60°, 30°, and 15°, respectively, and Rx HPBW of 15°. For an office environment and under LOS conditions values are 102° and 66.4° for a HPBW of 30° at both ends and 60° at both ends, respectively. For the office environment with NLOS, 60.2° and 22.2° is found for Tx-HPBW of 360° and 30°, respectively, in combination with an Rx-HPBW of 15°. These figures indicate that there is no clear relationship between angular spread and antenna beamwidth.

Next to angular spread, a characterization of cluster locations would be useful as they could be exploited by various beamforming or spatial diversity combining algorithms to enhance the system's performance [58]. Temporal-angular channel sounding measurements have been analyzed to determine whether ray arrivals at the receiver tend to form clusters in the 2-D time-angle space [59]. The obtained energy distribution among the clusters suggests that a single-cluster statistical model is probably sufficient to describe the channel behavior in LOS scenarios. Further results are required to verify this conjecture.

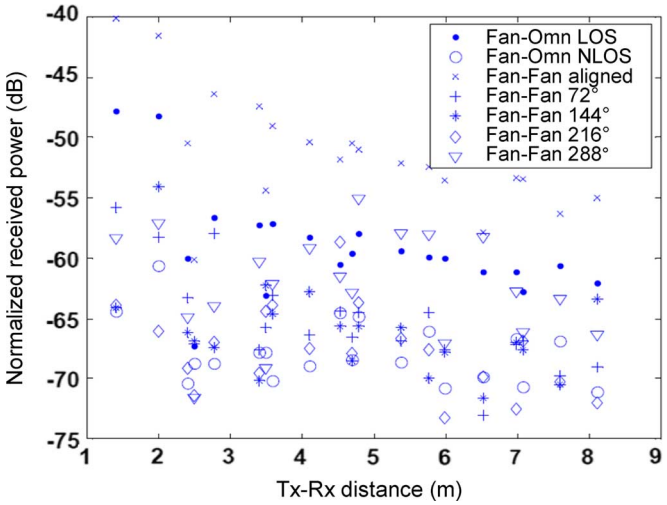

Fig. 5. Normalized received power as function of Tx-Rx distance. Tx antenna has a fan beam directed to the middle of the room. Rx antenna is omnidirectional with LOS (Fan-Omn LOS), omnidirectional with NLOS (Fan-Omn NLOS), Fan beam with 0° pointing error (Fan-Fan aligned), Fan beam with 72° mispointing (Fan-Fan 72°), Fan beam with 144° mispointing (Fan-Fan 144°), Fan beam with 216° mispointing (Fan-Fan 216°), Fan beam with 288° mispointing (Fan-Fan 288°).

- *TSV model*: A further elaboration of the S-V has been proposed in [57] and [60] denoted as the TSV model. In this model, a direct path component is added based on a two-path model and taking into account the directivity functions of the transmitting and receiving antenna. These references also provide a complete S-V model parameterization for office and residential environments.
- *Modeling of circular polarization*: The previously described models in this section are all based on linear polarization. As already indicated in Section II, it makes sense to incorporate the effects of circular polarization for LOS scenarios. This can be done by weighting each component in an impulse response with the probability that it will experience a significant cross polarization [61]. This may lead to a significant reduction in the amplitude of the indirect path signals [62] and as such in reduction of delay spread as reported in [47] and [63].
- *Further sophistication*: To date, angular spread and clustering is only measured and modeled in the azimuth plane. However, beamforming via ceilings etc. obviously requires modeling of angular spread and clustering in elevation as well. Furthermore, most research is limited to angle of arrival whereas the combination of angle of arrival and angle of departure is also interesting. Because of the complexity of these kind of measurements it might be practical to simulate this with calibrated ray-tracing software.

IV. Summary and Conclusions

This paper addresses the statistical characterization of indoor radio channels operating in the 60-GHz frequency band. It includes an overview of reported channel measurement and characterization activities. Large-scale fading as well as small-scale effects are taken into consideration.

Based on a large number of published measurement results a generic 60-GHz indoor radio channel model is proposed for

the large-scale fading. In addition, a large-scale fading model is proposed for the office environment in particular. It occurs that, with LOS, the path-loss exponent amounts to about 1.7 which is quite similar to what is found for conventional microwave frequencies.

As regards the characterization of small-scale effects we considered Doppler spread, delay spread and angular spread. From Doppler spread considerations it occurs that 60-GHz radios that support Gbps transmission encounter "slow fading". Delay spread considerations reveal that rms delay spread can be made very small, i.e., in the order of 1 ns, by using narrow-beam antennas. In addition, a considerable amount of mispointing can be tolerated when using fan beams. As regards angular spread the characterization of cluster locations is performed in order to enable optimization of beamforming algorithms and diversity combining algorithms. Based on these measurements a single cluster model is suggested for LOS situations.

It occurs that there is still a lack of available measurement data in particular with respect to the residential environment whereas the office environment might not be well representative for the home interior because of the presence of soft absorptive material of couches etc. Extensive measurement campaigns are required in this type of environment to chart out the large-scale as well as small-scale channel properties with in mind the uncompressed high-definition application requiring highly-directive channels. In particular, more angle-of-arrival data are needed, including clustering statistics. This also accounts for the office environment. Another important issue to be addressed urgently is polarization mismatch. The likely use of array antennas that produce linearly-polarized waves may yield a rather undefined direction of polarization at the receiving end whereas circular polarization may attenuate the one and only reliable reflection too much. This issue has to be investigated in detail, e.g., to motivate the choice between linear and circular polarization. As regards the fast download at short distance application, the use of circular polarization seems an obvious choice. Hence, the channel properties for this combination is also a prime topic for future research.

ACKNOWLEDGMENT

The author would like to thank the anonymous reviewers of this paper for their valuable suggestions.

REFERENCES

[1] P. Smulders, "Exploiting the 60 GHz band for local wireless multimedia access: Prospects and future directions," *IEEE Commun. Mag.*, vol. 40, no. 1, pp. 140–147, Jan. 2002.

[2] P. Smulders, H. Yang, and I. Akkermans, "On the design of low-cost 60-GHz radios for multigigabit-per-second transmission over short distances," *IEEE Commun. Mag.*, vol. 45, no. 12, pp. 44–51, Dec. 2007.

[3] H. Harada and I. Lakkis, Merged Proposal: New PHY Layer and Enhancement of MAC for mm Wave System Proposal, Doc. IEEE 802.15-07-0934-01-003c, IEEE P802.15 Working Group for WPANs, Nov. 2007 [Online]. Available: http://www.ieee802.org/15/pub/TG3c.html

[4] G. Baldwin *et al.*, Proposal for HD AV and Data Support, Doc. IEEE 802.15-07/942r2, IEEE P802.15 Working Group for WPANs, May 2007 [Online]. Available: http://www.ieee802.org/15/pub/TG3c.html

[5] WirelessHD, WirelessHD Specification Version 1.0 Overview, Res. Lab. Electron., Massachusetts Inst. Technol., Cambridge, MA, Oct. 2007 [Online]. Available: http://wirelesshd.org/, Tech. Rep.

[6] *High Rate 60 GHz PHY, MAC and HDMI PAL*, Standard ECMA-387, Ecma International, Dec. 2008 [Online]. Available: http://www.ecma-international.org/publications/standards/Ecma-387.htm

[7] E. Pearhia, VHT 60 GHz PAR Plus 5C's, Doc. IEEE 802.11-08/0806r7, IEEE P802.11 Working Group for WLANs, Nov. 2008 [Online]. Available: https://mentor.ieee.org/802.11

[8] H. Yang, P. F. M. Smulders, and M. H. A. J. Herben, "Indoor channel measurements and analysis in the frequency bands 2 GHz and 60 GHz," in *Proc. IEEE Symp. Pers. Indoor Mob. Radio Commun.*, 2005, pp. 1–5.

[9] A. Sadri, 802.15.3c Usage Model Document, Doc. IEEE 802.15-06-0055-21-003c, IEEE P802.15 Working Group for WPANs, 2006.

[10] S. Kato, "R&D on millimeter wave (60 GHz) systems and IEEE standardization updates," in *Proc. IEEE Int. Conf. Ultra-Wideband*, 2007, pp. 514–517.

[11] D. C. Cox, R. Murray, and A. Norris, "800 MHz attenuation measured in and around suburban houses," *AT&T Bell Lab. Tech. J.*, vol. 673, no. 6, Jul.–Aug. 1984.

[12] R. C. Bernhardt, "Macroscopic diversity in frequency reuse systems," *IEEE J. Sel. Areas Commun.*, vol. SAC-5, pp. 862–878, Jun. 1987.

[13] M. Jacob and T. Kürner, "Radio channel characteristics for broadband WLAN/WPAN applications between 67 and 110 GHz," in *Proc. Eur, Conf. Antennas and Propag.*, Berlin, Germany, Mar. 2009, pp. 2663–2667.

[14] H. Xu, V. Kukshhya, and T. S. Rappaport, "Spatial and temporal characteristics of 60-GHz indoor channels," *IEEE J. Sel. Areas Commun.*, vol. 20, no. 3, pp. 620–630, Apr. 2002.

[15] M. Fryziel, C. Loyer, L. Clavier, N. Rolland, and P. A. Rolland, "Path-loss model of the 60-GHz indoor radio channel," *Microw. Opt. Lett.*, vol. 34, no. 3, pp. 158–162, 2002.

[16] T. Zwick, T. J. Beukema, and H. Nam, "Wideband channel sounder with measurements and model for the 60 GHz indoor radio channel," *IEEE Trans. Veh. Technol.*, vol. 54, no. 4, pp. 1266–1276, Jul. 2005.

[17] S. Geng, J. Kivinen, X. Zhao, and P. Vainikainen, "Millimeter-wave propagation channel characterization for short-range wireless communications," *IEEE Trans. Veh. Technol.*, vol. 58, no. 1, pp. 3–13, Jan. 2009.

[18] M. Peter and W. Keusgen, "Analysis and comparison of indoor wideband radio channels at 5 and 60 GHz," in *Proc. European Conf. Antennas and Propag.*, Berlin, Germany, Mar. 2009, pp. 3830–3834.

[19] H. Yang, P. F. M. Smulders, and M. H. A. J. Herben, "Channel characteristics and transmission performance for various channel configurations at 60 GHz," *EURASIP J. Wireless Commun. Netw.*, 2007, Article ID 19613, 15 pages.

[20] J. Kivinen, "60-GHz wideband radio channel sounder," *IEEE Trans. Instrum. Meas.*, vol. 56, no. 5, pp. 1831–1838, Oct. 2007.

[21] S. Collonge, G. Zaharia, and G. E. Zein, "Wideband and dynamic characterization of the 60 GHz indoor radio propagation—Future home WLAN architectures," *Ann. Télécommun.*, vol. 58, no. 3–4, pp. 417–447, 2004.

[22] D. M. Matic, H. Harada, and R. Prasad, "Indoor and outdoor frequency measurements for mm-waves in the range of 60 GHz," in *Proc. IEEE Vehicular Technology Conf.*, 1998, pp. 567–571.

[23] P. Nobles and F. Halsall, "Indoor propagation at 17 GHz and 60 GHz-measurements and modeling," in *Proc. Nat. Conf. Antennas and Propag., IEE Conf. Pub.*, 1999, no. 461, pp. 93–96.

[24] C. R. Anderson and T. S. Rappaport, "In-building wideband partition loss measurements at 2.5 and 60 GHz," *IEEE Trans. Wireless Commun.*, vol. 3, no. 3, pp. 922–928, May 2004.

[25] S.-K. Yong, TG3c Channel Modeling Sub-Committee Final Rep., Doc. IEEE P802.15-07-0584-01-003c, IEEE P802.15 Working Group for WPANs, Mar. 2007 [Online]. Available: http://www.ieee802.org/15/pub/TG3c.html

[26] P. Pagani, N. Malhouroux, I. Siaud, and V. Guillet, Characterization and Modeling of the 60 GHz Indoor Channel in the Office and Residential Environments, Doc. IEEE P802.15-06-0027-01-003c, IEEE P802.15 Working Group for WPANs, Jan. 2006.

[27] T. S. Rappaport, *Wireless Communications: Principles and Practice*, 2nd ed. Upper Saddle River, NJ: Prentice-Hall, 2002, p. 139, 0-13-042232-0.

[28] S. Collonge, G. Zaharia, and G. E. Zein, "Influence of furniture on 60-GHz radio propagation in a residential environment," *Microw. Opt. Technol. Lett.*, vol. 39, no. 3, pp. 230–233, Nov. 2003.

[29] M. Peter and W. Keusgen, "Impact of antenna configuration and shadowing on the characteristics of the 60 GHz indoor wideband radio channel," presented at the URSI General Assembly, Chicago, IL, Aug. 2008.

[30] K. Sato and T. Manabe, "Estimation of propagation-path visibility for indoor wireless LAN systems under shadowing conditions by human bodies," in *Proc. IEEE 48th Vehicular Technology Conf.*, May 1998, vol. 3, pp. 2109–2113.
[31] S. Collonge, G. Zaharia, and G. E. Zein, "Influence of the human activity on wideband characteristics of the 60 GHz indoor radio channel," *IEEE Trans. Wireless Commun.*, vol. 3, no. 6, pp. 2396–2406, Nov. 2004.
[32] P. F. M. Smulders, "Broadband Wireless LANs: A Feasibility Study," Ph.D. dissertation, Eindhoven Univ. Technol., Eindhoven, The Netherlands, 1995, 90-386-0100-X.
[33] P. A. Bello, "Characterization of randomly time-variant linear channels," *IEEE Trans. Commun. Syst.*, vol. CS-11, no. 12, pp. 360–393, Dec. 1963.
[34] K. Witrisal, Y.-H. Kim, and R. Prasad, "Frequency-domain simulation and analysis of the frequency-selective Ricean fading radio channel," in *Proc. IEEE 9th Symp. Pers. Indoor Mobile Radio Commun.*, Sep. 1998, pp. 1131–1135.
[35] N. Moraitis, "Measurements and characterization of wideband indoor radio channel at 60 GHz," *IEEE Trans. Wireless Commun.*, vol. 5, no. 4, pp. 880–889, Apr. 2006.
[36] W. Sawaya and L. Clavier, "Simulation of DS-CDMA on the LOS multipath 60 GHz channel and performance with RAKE receiver," in *Proc. IEEE 14th Symp. Pers. Indoor Mobile Radio Commun.*, 2003, pp. 1232–1236.
[37] R. H. Clarke, "A statistical theory of mobile-radio reception," *Bell Syst. Tech. J.*, vol. 47, no. 6, pp. 957–1000, 1968.
[38] R. H. Clarke and W. L. Khoo, "3-D mobile radio statistics," *IEEE Trans. Veh. Technol.*, vol. 46, no. 3, pp. 798–799, Mar. 1997.
[39] S. Guillouard, G. E. Zein, and J. Citerne, "Wideband propagation measurements and Doppler analysis for the 60 GHz indoor channel," in *Proc. IEEE MTT-S Dig.*, 1999, pp. 1751–1754.
[40] N. Moraitis and P. Constantinou, "Indoor channel measurements and characterization at 60 GHz for wireless local area network applications," *IEEE Trans. Antennas Propag.*, vol. 52, no. 12, pp. 3180–3189, Dec. 2004.
[41] K. Witrisal, G. Landman, and Bohdanowicz, "Practical application of novel method for estimating the RMS delay spread from power measurements," presented at the 4th Eur., Mobile Commun. Conf., Vienna, Austria, Feb. 2001.
[42] C. Liu, E. Skafidas, T. S. Pollock, and R. J. Evans, "Angle of arrival extended S-V model for the 60 GHz wireless desktop channel," presented at the IEEE Symp. Pers. Indoor Mob. Radio Commun., 2006.
[43] A. A. M. Saleh and R. A. Valenzuela, "A statistical model for indoor multipath propagation," *IEEE J. Sel. Areas Commun.*, vol. SAC-5, no. 2, pp. 128–137, Feb. 1987.
[44] J.-H. Park, Y. Kim, Y.-S. Hur, K. Lim, and K.-H. Kim, "Analysis of 60 GHz band indoor wireless channels with channel configurations," in *Proc. IEEE 9th Symp. Pers. Indoor Mobile Radio Commun.*, Sep. 1998, vol. 2, pp. 617–620.
[45] P. F. M. Smulders and A. G. Wagemans, "Biconical horn antennas for near uniform coverage in indoor areas at mm-wave frequencies," *IEEE Trans. Veh. Technol.*, vol. 43, no. 4, pp. 897–901, Nov. 1994.
[46] P. F. M. Smulders and A. G. Wagemans, "Frequency-domain measurement of millimeter wave indoor radio channel," *IEEE Trans. Instrum. Meas.*, vol. 44, no. 6, pp. 1017–1022, Dec. 1995.
[47] T. Manabe, K. Sato, H. Masuzawa, K. Taira, T. Ihara, Y. Kasashima, and K. Yamaki, "Polarization dependence of multipath propagation and high-speed transmission characteristics of indoor millimeter-wave channel at 60 GHz," *IEEE Trans. Veh. Technol.*, vol. 44, no. 2, pp. 268–273, May 1995.
[48] H. Yang, P. F. M. Smulders, and M. H. A. J. Herben, "Frequency selectivity of 60 GHz LOS and NLOS indoor radio channels," in *Proc. IEEE Vehicular Technology Conf.*, Melbourne, Australia, 2006, pp. 2727–2731.
[49] P. F. M. Smulders, M. H. A. J. Herben, and J. George, "Application of five-sector beam antenna for 60 GHz wireless LAN," *Electron. Lett.*, vol. 38, no. 18, pp. 1054–1055, Aug. 2002.
[50] H. Yang, M. H. A. J. Herben, J. A. G. Akkermans, and P. F. M. Smulders, "Impact analysis of directional antennas and multiantenna beamformers on radio transmission," *IEEE Trans. Veh. Technol.*, vol. 57, no. 3, pp. 1695–1707, May 2008.
[51] H. Yang, "Towards Low-Cost Gigabit Wireless Systems at 60 GHz: Channel Modelling and Baseband Design," Ph.D. dissertation, 978-90-386-1425-0, 2008.
[52] P. F. M. Smulders and L. M. Correia, "Characterisation of propagation in 60 GHz radio channels," *Electron. Commun. Eng. J.*, pp. 73–80, Apr. 1997.
[53] Q. Spenser, B. Jeffs, M. Jensen, and A. Swindlehurst, "Modeling the statistical time and angle of arrival characteristics of an indoor multipath channel," *IEEE J. Sel. Areas Commun.*, vol. 18, no. 3, pp. 347–360, Mar. 2000.
[54] C.-C. Chong, C.-M. Tan, D. Laurenson, S. McLaughlin, M. Beach, and A. Nix, "A new statistical wideband spatio-temporal channel model for 5 GHz band wlan systems," *J. Sel. Areas Commun.*, vol. 21, no. 2, pp. 139–150, 2003.
[55] T. Kürner and M. Jacob, "Application of ray tracing to derive channel models for future multi-gigabit systems," presented at the 11th Int. Conf. Electromagnetics in Advanced Applicat., Turin, Italy, Sep. 2009.
[56] M.-S. Choi, G. Grosskopf, and D. Rohde, "Statistical characteristics of 60 GHz wideband indoor propagation channel," presented at the IEEE 16th Symp. Pers. Indoor Mobile Radio Commun., Berlin, Germany, Sep. 2005.
[57] K. Sato, H. Sawada, Y. Shoji, and S. Kato, "Channel model for millimeter wave WPAN," presented at the IEEE Symp. Pers. Indoor Mob. Radio Commun., 2007.
[58] B. Neekzad, K. Sayrafian-Pour, and J. S. Baras, "Energy efficient millimeter wave radio link establishment for low probability of intercept with smart antenna," presented at the 25th Army Science Conf., Orlando, FL, Nov. 2006.
[59] B. Neekzad, K. Sayrafian-Pour, and J. S. Baras, "Clustering characteristics of millimeter wave indoor channels," presented at the IEEE Wireless Communications Networking Conf., Los Angeles, CA, Mar.–Apr. 2008.
[60] H. Sawada, Y. Shoij, C.-S. Choi, K. Sato, R. Funada, H. Harad, S. Kato, M. Umehira, and H. Ogawa, Merging Two-Path and S-V Models for LoS Desktop Channel Environments, Doc. 802.15-06-0297-02-003c, IEEE Working Group for WPANs, 2006.
[61] F. Yildirim, A. S. Sadri, and H. Liu, "Polarization effects for indoor wireless communications at 60 GHz," *IEEE Commun. Lett.*, vol. 12, no. 9, pp. 660–662, Sep. 2008.
[62] C. Loyez, N. Rolland, P. A. Rolland, and O. Lafond, "Indoor 60 GHz radio channel sounding and related T/R module considerations for high data rate communications," *Electron. Lett.*, vol. 37, no. 10, p. 654, May 2001.
[63] T. Manabe, Y. Miura, and T. Ihara, "Effects of antenna directivity and polarization on indoor multipath propagation characteristics at 60 GHz," *IEEE J. Sel. Areas Commun.*, vol. 14, no. 3, pp. 441–448, Apr. 1996.

Peter F. M. Smulders (S'83–M'85–SM'96) graduated from Eindhoven University of Technology (TU/e), Eindhoven, The Netherlands, in 1985. He performed Ph.D. research in the field of broadband wireless LANs and received the Ph.D. degree in 1995. In his Ph.D. studies, he addressed the feasibility of broadband wireless LANs operating at 60 GHz.

In 1985, he joined the Propagation and Electromagnetic Compatibility Department of the Research Neher Laboratories of the Netherlands PTT. During that time, he was doing research in the field of compromising emanation from civil data processing equipment. In 1988, he moved to the TU/e as a staff member of the Telecommunications Division. He was involved in various research projects addressing 60-GHz channel characterization (COST 231), 60-GHz antennas and interworking (ACTS, MEDIAN), and 60-GHz channel characterization and baseband design (MinEZ, Broadband Radio@Hand and Freeband WiComm). Currently, he is with the Electromagnetics and Wireless Group of TU/e as an Associate Professor. Next to his lecturing duties, his current work addresses integral system design of low-cost, low-power, small-sized wireless LAN/PAN technology operating in the 60-GHz band. As a participant of the Medea+ project Q-Stream, he addresses antenna and propagation issues. As a project manager of the IOP GenCom project SiGi-Spot, his research activities range from 60-GHz physical-layer design to associated network aspects. His field of interest that covers channel modeling, front-end technology including antennas, modulation and coding and MAC and higher layers is reflected in numerous IEEE publications.

Dr. Smulders is presently a board member of the J. C. Maxwell foundation. He is a Guest Editor for the EURASIP *Journal on Wireless Communications and Networking*. He is also member of the Royal Institute of Engineers (KIvI) and the Netherlands Electronics and Radio Society (NERG).